CBPF-NF-060/96

Magnetism, Chemical Bonding and Hyperfine Properties in the Nanoscale Antiferromagnet $[Fe(OMe)_2(O_2CCH_2Cl)]_{10}$

Z. Zeng[+], *Y. Duan* and *Diana Guenzburger*[*]

Centro Brasileiro de Pesquisas Físicas - CBPF
Rua Dr. Xavier Sigaud, 150
22290-180 – Rio de Janeiro, RJ – Brasil

Abstract

The electronic and magnetic properties of the nanometer-size antiferromagnet $[Fe(OMe)_2(O_2CCH_2Cl)]_{10}$ (the "ferric wheel" molecule) are investigated with the first-principles spin-polarized Discrete Variational Method, in the framework of Density Functinal theory. Magnetic moments, densities of states and charge and spin-density maps are obtained. The Mössbauer hyperfine parameters Isomer shift, Quadrupole Splitting and Hyperfine Field are obtained from the calculations and compared to reported experimental values when available.

Key-words: Antiferromagnet; Hyperfine parameters; Nanoscale.

[+]On leave from: Institute of Solid-State Physics, Academia Sinica, Hefei 230031, People's Republic of China.

[*]Author to whom correspondence should be addressed. e-mail: DIANA@CBPFSU1.CAT.CBPF.BR

1 Introduction

In recent years, there has been considerable effort in constructing and investigating the properties of systems of nanoscale or mesoscopic dimensions, containing a finite number of magnetic transition-metal atoms [1]. Such systems may be considered to be in the borderline of isolated and collective magnetic behaviour, displaying characteristics of both types. Moreover, new and exciting magnetic effects are expected to appear [2].

There are several techniques for obtaining mesoscopic clusters of transition metal atoms. $Fe(CO)_5$ was decomposed by a scanning tunneling microscope to form Fe particles on a semiconductor or metal substrate [3]. Particles of about 20nm of an Fe-Ni alloy were obtained by lithography [4]. Nanocrystalline γ-Fe_2O_3 with particle sizes of the order of $100\mathring{A}$ has been obtained as a polymer nanocomposite [5]. The magnetic protein ferritin consists of a core of hydrated Fe_2O_3 containing $\sim$4500 Fe^{3+} ions, surrounded by a spherical polypeptide shell [6]; magnetite (Fe_3O_4) particles of nanoscopic dimensions were synthetized within the polypeptide cavity [7].

However, procedures of the type above do not allow the control of the size of the particles yielding clusters of dimensions within a range of values. Systems with well-determined numbers of magnetic atoms may be obtained by chemical synthesis of large polynuclear organo-metallic molecules [8]-[16]. These are usually constituted of a core of transition-metal atoms bridged by Oxygen (or S), surrounded by organic ligands. The molecules may cling together by van der Waals forces forming crystals of well-defined structures; however, the organic ligands that encapsulate the magnetic cores prevent interactions between molecules at the distances founds. Thus magnetic ordering effects observed will be entirely due to interactions within the molecule.

Nanometer-scale systems of dimensions below $\sim$20nm may exhibit interesting effects [2]. For such small number of spins, the whole cluster constitutes one sole magnetic domain either ferromagnetic (FM) or antiferromagnetic (AFM). If the direction of magnetization fluctuates in time between two orientations, the system is superparamagnetic. For Fe clusters, superparamagnetism may be studied by Mössbauer spectroscopy; this has been reported for ferritin [17] and for oxo-Fe clusters with organic ligands [11]. Tunneling between the two superparamagnetic states may also occur, and has been detected in ferritin [6].

Important new technological applications may be envisaged for these nanoscale magnetic systems, due to their remarkable properties. Pronounced hysteresis in the magnetization of a Mn_{12} cluster compound was reported; such bistable magnetic molecule could act as a data storage device [18]. Theoretical predictions suggest that superparamagnetic materials may exceed the performance of the currently used paramagnetic compounds in magnetic refrigeration [19]. Particles of γ-Fe_2O_3 have been found to be considerably more transparent to visible light than the single-cristal from, thus combining interesting magnetic and optical properties due to nanoscale dimensions [5]. Finally, the properties of oxo-Fe clusters are attracting considerable attention as these form models for ferritin, of great biological importance and potential use in magnetic resonance imaging [1].

Electronic structure calculations for these systems will allow the understanding of their magnetic and electronic properties at the microscopic level. Calculations for a Fe_6-cluster molecule with the xα-Scattered Wave method have been reported [16]. Here we

focus on the circular molecule $[Fe(OMe)_2(O_2CCH_2Cl)]_{10}$ denominated "ferric wheel" [9], [10]; magnetization and susceptibility measurements reveal it to be a perfect molecular antiferromagnet with an S =0 quantum ground state. The molecules are arranged in a crystalline structure in which the units are sufficiently distant to preclude magnetic interactions among them. It has been suggested by a theoretical study that antiferromagnetic nanosize particles are better candidates for observation of superparamagnetic tunneling [20]. Moreover , Mössbauer hyperfine parameters have been measured [10].

A transition-metal molecule of this size constitutes a challenge for present day electronic-structure methods. We have employed the first-principles numerical Discrete Variational method (DVM) based on Density Functional Theory (DFT) to study the AFM ground-state properties of the ferric-wheel. The method will be briefly described in Section 2, the results reported and analysed in Section 3 and 4, and conclusions summarized in Section 5.

2 Theoretical Method

In the Discrete Variational method [21], the Kohn-Sham equations [22] of Density Functional theory are solved self-consistently, for a cluster of atoms or a molecule in a three-dimensional grid of points (in hartrees):

$$(-\nabla^2/2 + V_c + V_{xc}^{\sigma})\phi_{i\sigma} = \varepsilon_{i\sigma}\phi_{i\sigma} \tag{1}$$

In Eq. (1), V_c is the Coulomb potential of nuclei and electrons, and V_{xc}^{σ} is the exchange and correlation potential [23] which is a functional of the electron density of spin σ:

$$\rho_{\sigma}(\vec{r}) = \sum_i n_{i\sigma}|\phi_{i\sigma}(\vec{r})|^2 \ . \tag{2}$$

$\phi_{i\sigma}$ are the one-electron molecular functions and $n_{i\sigma}$ their occupation, given by Fermi-Dirac statistics. In the present spin-polarized calculations, the electron density for spin $\uparrow$ is free to be different from spin $\downarrow$, thus allowing the exchange interaction to generate a spin density $[\rho_{\uparrow}(\vec{r}) - \rho_{\downarrow}(\vec{r})]$.

The molecular spin orbitals $\phi_{i\sigma}$ are expanded as a linear combination of numerical atomic functions. The atomic functions of this basis are obtained by self-consistent (SCF) DFT atomic calculations. The DV method leads to secular equations which are solved self-consistently in the three-dimensional grid:

$$([H] - [E][S])[C] = 0 \tag{3}$$

In Eq. (3), [H] is the Kohn-Sham hamiltonian matrix, [S] the overlap matrix and [C] the matrix of the coefficientes which define $\phi_{i\sigma}$.

To facilitate the calculation of the electron-electron interaction, a model potential is constructed by fitting the charge density to a multicenter multipolar expansion [24], with variational coefficients obtained by a least-squares fit to the "true" density. The multipoles may have any order needed; however, in the present calculation only spherical terms were retained due to the size of the system. This is expected to be sufficiently accurate to describe the approximately spherical Fe cations.

The numerical grid was pseudo-random (Diophantine) [21] except inside spheres centered at the Fe nuclei, where a more precise polynomial integration is necessary, due to oscillations of the core functions. The total number of points per atom was: Fe 5,550, O 420, C 420. For each Fe atom, 5,050 points are inside the sphere of 1.5 a.u. and 500 are diophantine. Several hundred potential iterations were performed to achieve self-consistency of <0.01 in $\rho(\vec{r})$.

A Mulliken-type population analysis [25] was performed to obtain the atomic configurations of the atoms in the molecule. Thus magnetic moments were defined as the difference between spin up and spin down populations. The atomic basis was formed by Fe 3s, 3p, 3d, 4s, 4p, O 2s, 2p and C 2s, 2p. The inner orbitals were kept frozen throughout the SCF calculations, after beeing explicitly orthogonalized against the valence basis. Improvement of the basis is achieved by generating new functions obtained with SCF calculations for atoms with orbital occupations approximately the same as obtained for the molecule.

The computer programs employed were the DVM codes developed at Northwestern University.

3 Electronic Structure, Magnetism and Chemical Bond

To render the problem tractable, we disregarded the terminal H and Cl atoms, located at the extremities of bonds. In this way, the number of atoms was reduced to 90 and D_5 point symmetry was preserved for the AFM ground state. The resulting cluster $[Fe(OC)_2(O_2CC)]_{10}$ representing the "ferric wheel" molecule is depicted in Figs. 1a and 1b. Interatomic distances and angles were obtained from experiment [9], [10]. Small deviations from average values were disregarded, to preserve D_5 symmetry.

In Fig. 2 is shown a map of the total electron density on the plane of the Fe atoms ($z = 0$), and in Fig. 3, a map of the spin-density $[\rho_\uparrow(\vec{r}) - \rho_\downarrow(\vec{r})]$ of the Fe atoms. The spin density around each Fe is slightly elongated in the radial direction, probably due to Pauli repulsion. In Table I are given the Fe Mulliken populations (occupations of atomic orbitals) and magnetic moments μ obtained for the molecule. The net charge found for Fe is +2.3. The 4s and 4p orbitals have very small populations, due to charge transfer to the neighbor Oxygens; however, the 3d$\downarrow$ orbital has the non-negligible occupation of 0.6 electrons, and so the magnetic moment on Fe is $4.3\mu_B$, smaller than the $5\mu_B$ of a Fe^{3+} ion.

Due to the truncation of the C−H and C−Cl bonds, as small spurious fractional spin moment is obtained on the terminal Carbons. However, they have not affected the results for Fe to any significant extent, as the neighboring Oxigens have $\sim$ zero spin moments.

To compare with the molecule, we have performed an SCF calculation for a ring of ten Fe atoms, at the same positions as in the molecule. The results are also given in Table I. Due to the absence of the electron-attracting Oxygen atoms, the 4s and 4p, as well as 3d$\downarrow$, orbitals of Fe have considerably larger occupations, resulting in a total reduced moment ($3.7\mu_B$). However, this moment is still considerably larger than the value for bulk α−Fe ($2.2\mu_B$). This indicates that the geometrical arrangements and interatomic distances of the Fe_{10} cluster play an important role in bringing about a large magnetic moment on Fe.

The eigenvalues ε_i of Eq. 1 form a dense band of discrete energy levels. As is defined for a solid, Partial Density of States (P DOS) diagrams may be constructed by broadening the levels with Lorentzians [26]:

$$D^q_{n\ell\sigma}(\varepsilon) = \sum_i P^q_{n\ell\sigma i} \; \frac{\delta/\pi}{(\varepsilon - \varepsilon_{i\sigma})^2 + \delta^2} \tag{4}$$

where $P^q_{n\ell\sigma i}$ is the Mulliken population of atomic orbital $\chi_{n\ell}$ of atom q in the molecular spin-orbital $\phi_{i\sigma}$, and δ is the half-width of the Lorentzian, here taken as 0.136 eV. By summing over n, ℓ and i the local DOS of spin σ for atom q is obtained; summing over all atoms and σ gives the total DOS.

The total DOS for the molecule is shown in Fig. 4. The occupied energy levels span a large interval of about 22 eV, from the deeper 2s levels of Oxygen to the antibonding Fe 3d. In Fig. 5 we can see the PDOS for the Fe 3d orbital. The 3d↑ levels form a very narrow band located at about 4eV below the "Fermi level" (or HOMO, highest occupied molecular orbital), and a broad structure at lower energies due to bonding.

The "Fermi level" crosses the lower part of the 3d↓ band, which shows several peaks, also due to chemical interaction. In Figs. 6a and 6b are displayed the PDOS of Fe 4s and 4p; we can see very small peaks where participation in bonding occurs, but mostly empty levels, consistent with the small populations in Table I.

We have investigated the nature of the bonding forces that draw together this remarkable molecule, by calculating from the functions $\phi_{i\sigma}$ the bond orders of the Fe bonds with its neighbors, given in Table II. Considering the linear expansion of $\phi_{i\sigma}$ in the atomic orbitals, the bond order (B.O.) of the bond between atoms p and q is defined as:

$$B.O. = \sum_{i,\sigma} \sum_{k,m} n_{i\sigma} \; c^*_{ik\sigma} c_{im\sigma} S_{km} \tag{5}$$

$$S_{km} = \int \chi^*_k \chi_m \, dv$$

where S_{km} is the overlap integral between basis functions χ_k and χ_m centered at atoms p and q respectively. It is seen in Table II that most of the Fe bonds with its neighbor atoms have very small or negative bond orders, signifying non-bonding or antibonding interactions. The only exception is the Fe bond with the C in the Fe–O–C–O–Fe bridge (atom no. 9 in Fig. 7), which has a bond order of ∼0.14 and thus contributes to the covalent stabilization of the Fe ring. The C and O atoms form covalent bonds among themselves; but most of the stabilizing forces involving the Fe cations are thus the eletrostatic interactions with the Oxygen anions.

4 Hyperfine interactions

The Mössbauer spectrum of polycrystalline $[Fe(OMe)_2(O_2CCH_2Cl)]_{10}$ at 4.2 K has been measured, and the parameters Isomer shift (δ) and Quadrupole Splitting (Δ EQ) derived [10].

The Isomer shift is defined as [27], [28]:

$$\delta = 2/3 \; e^2 \pi Z S'(Z) \Delta < r^2 > [\rho_A(0) - \rho_S(0)] \equiv \alpha \Delta\rho(0) \tag{6}$$

where $\Delta < r^2 >$ is the variation of the mean square radius of the nucleus between excited and ground states of the Mössbauer transition, $S'(Z)$ is a correction for relativistic effects, and the term is brackets is the difference between the electron density at the nucleus in the absorber A and source S (in other words, between a given compound and a standard system). As defined, δ is linear against $\rho(0)$ for a series of compounds or ionic states of Fe. In a non-relativistic appproximation, only orbitals containing s-states of Fe contribute to $\rho(0)$.

In the course of calculating δ for the molecule $FeNH_3$, the constant α containing nuclear parameters that multiplies $\Delta\rho(0)$ in Eq. 6 has been derived by plotting δ and $\rho(0)$ for the Fe atom and ions [29]. $\rho(0)$ did not include the 1s and 2s contributions of Fe, since these practically do not vary from one compound to another. From this plot, the equation $\delta = -0.228\rho(0)+33.638$ is obtained, which allows the derivation of δ for the present molecule. The value is given in Table III, where it is compared to experiment. The positive sign of δ means a smaller electron density at the nucleus than the standard compound, Fe metal, consistent with the small 4s population (Table I) and the charge +2.3.

The quadrupole splitting ΔEQ of the excited state of the 14.4 keV transition of ^{57}Fe is given by:

$$\Delta EQ = 1/2\ eV_{zz}Q\left(1+\frac{\eta^2}{3}\right)^{1/2} \tag{7}$$

where Q is the quadrupole moment of the nucleus in the excited state (I= 3/2), V_{zz} the electric field gradient and η the asymetry parameter.

The electric field gradient is produced by the non-spherical charge distribution of the nuclei and electrons around the probe nucleus. It is a traceless tensor whose components are defined as

$$V_{ij} = \frac{\partial^2 V}{\partial x_i \partial x_j}\ (x_i, x_j = x, y, z) \tag{8}$$

where V is the eletrostatic potential. Each one of the six independent components of the symmetric tensor was calculated with the expression (in atomic units) [29] -[32]:

$$V_{ij} = -\int \rho(\vec{r})(3x_i x_j - \delta_{ij}r^2)/r^5 dv + \sum_q Z_q^e(3x_{qi}x_{qj} - \delta_{ij}r_q^2)/r_q^5 \tag{9}$$

The first term Eq. 9 is the electronic contribution, obtained with the molecular $\rho(\vec{r})$, and the second term the contribution of the surrounding nuclei shielded by the core electrons, with effective charge Z_q^e. After diagonalization, the electric field gradient is defined by the convention:

$$|V_{zz}| > |V_{yy}| \geq |V_{xx}| \tag{10}$$

with the asymetry parameter η given by:

$$\eta = \frac{V_{xx} - V_{yy}}{V_{zz}} \tag{11}$$

The eigenvectors obtained from the diagonalization define the direction of V_{zz}. In Table III are shown the diagonal components, the parameter η and the calculated value of ΔEQ. To obtain the latter, the value Q =0.16b was employed, as derived recently from accurate band-structure calculations for several Fe compounds [33]. In Table III the experimental value of ΔEQ is given for comparison. The sign was not determined experimentally; from the calculation, it is seen to be positive. V_{zz} for each Fe is mostly in the z direction, but tilted towards the neighbor Fe atoms. In Fig. 8 is given a schematic representation of the projection of V_{zz} on the $z = 0$ plane; for each Fe atom, it is perpendicular to the radius of the ring.

The Contact (or Fermi) component H_c of the magnetic hyperfine field at the Fe nucleus may be expected to be by far the largest in the present compound. H_c is proportional to the spin density at the Fe nucleus.

$$H_c = (8\pi/3) g_e \mu_B [\rho_\uparrow(0) - \rho_\downarrow(0)] \times \frac{1}{2} \tag{12}$$

We have calculated H_c and the value is given in Table IV. The core (1s−3s) and valence contributions are calculated separately: the valence spin density is obtained from the molecular calculation, and the core from an atomic calculation for an atom with the same configuration for Fe as it has in the molecule. The reason for this procedure is the lack of sufficient flexibility of the basis to polarize the core adequately.

We notice that the hyperfine field is dominated by the negative core contribution, as expected for the Fe ion with charge +2.3. The small valence component is consistent with the 4s population (0.09, Table I).

No magnetic hyperfine splitting was observed in the spectrum [10] measured at 4.2 K. This may possibly be ascribed to superparamagnetic fluctuations, at a rate faster than the Mössbauer transition time ($\sim 10^8$sec). More experiments at different temperatures and/or in the presence of an applied field would be necessary to clarify this aspect further [11]. The magnitude of the field (434 kG) is not far from the values measured for the similar (FM) nanoscale Fe_{11} and $Fe_{16}Mn$ oxo-organic agreagates (430 and 400 kG respectively) [11] but is smaller than the value for bulk $\alpha-Fe_2O_3$ (515 kG at room temperature [27]). The valence contribution to H_c in Fe may be positive (as in the present case) or negative, whereas the core contribution is always negative. Since the valence contribution is very small (see Table IV), and the core contribution results from the polarization of the core s electrons by the 3d magnetic moment, being proportional to this moment, this implies that μ(Fe) in the present molecule is smaller than in $\alpha-Fe_2O_3$.

5 Conclusions

With the spin-polarized Discrete Variational method, the electronic structure of the molecular antiferromagnet $[Fe(OMe)_2(O_2CCH_2Cl)]_{10}$ was investigated. A magnetic moment of $4.3\mu_B$ and charge +2.3 were found on the Fe. Analysis of the bond-order of the bonds with Fe reveals that only a Fe-C bond contributes to covalent stabilization of the molecule. Calculated values for the isomer shift δ and the quadrupole interaction ΔEQ compare well with experimental values reported. The sign and direction of the electric field gradient were determined; the calculated value of the magnetic hyperfine

field indicates that the magnetic moment on Fe in the present system is smaller than in $\alpha-Fe_2O_3$.

Acknowledgements

Calculations were performed at the Cray YMP of the Supercomputing Center of the Federal University of Rio Grande do Sul, and at the the Cray J90 of the Federal University of Rio de Janeiro (COPPE). This work was supported in part by RHAE – New Materials project no. 610195/92-1.

Table Captions

Table 1

Mulliken-type populations, net charges and magnetic moments μ of Fe in clusters $[Fe(OC)_2(O_2CC)]_{10}$ and Fe_{10}. Magnetic moments are for Fe atoms with positive spin.

Table 2

Bond-orders for Fe bonds in cluster $[Fe(OC)_2(O_2CC)]_{10}$. Atoms numbered according to Fig. 7.

Table 3

^{57}Fe electric hyperfine parameters of $[Fe(OC)_2(O_2CC)]_{10}$. Values of the isomer shift δ relative to Fe metal.

a) From reference [10].

b) Q(^{57}Fe)=0.16b (from reference [33]).

Table 4

Calculated magnetic hyperfine field H_c at the Fe nucleus.

Table I

	$[Fe(OC)_2(O_2CC)]_{10}$		Fe_{10}	
	Population	$\mu(\mu_B)$	Population	$\mu(\mu_B)$
3d	5.44	4.24	6.70	3.24
4s	0.09	0.04	1.19	0.36
4p	0.15	0.02	0.12	0.06
	net charge: +2.32	Total 4.30	Net charge: 0.0	Total 3.66
	$\uparrow$ $(m_s = 1/2)$	$\downarrow$ $(m_s = -1/2)$	$\uparrow$	$\downarrow$
3d	4.84	0.60	4.97	1.73
4s	0.07	0.03	0.78	0.42
4p	0.09	0.07	0.09	0.03

Table II

Fe(1)−Fe(2)	– – – – – – – – –	−0.001
Fe(1)−O(3)	– – – – – – – – –	+0.015
Fe(1)−C(4)	– – – – – – – – –	−0.020
Fe(1)−O(5)	– – – – – – – – –	+0.006
Fe(1)−C(6)	– – – – – – – – –	−0.014
Fe(1)−O(7)	– – – – – – – – –	+0.030
Fe(1)−O(8)	– – – – – – – – –	−0.001
Fe(1)−C(9)	– – – – – – – – –	+0.137
Fe(1)−C(10)	– – – – – – – – –	−0.005

Table III

Isomer Shift

$\rho(0)(a_0^{-3})$ (3s+valence)	δ(mm/s) (calculated)	δ(mm/s) (experimental)[a]
145.43	0.48	0.52

Electric field gradient

V_{zz} (a_0^{-3})	V_{yy} (a_0^{-3})	V_{xx} (a_0^{-3})	η	ΔE_Q(mm/s) (calculated)[b]	$\lvert\Delta E_Q\rvert$(mm/s) (experiment)[a]
0.439	−0.311	−0.128	0.416	+0.73	0.62

Table IV

	$\Delta\rho(0)$ (a_0^{-3})	H_c (kG)
1s−3s	−0.906	−474
valence	+0.077	+40
Total	−0.829	−434

Figure Captions

Figure 1a) Top view of the molecule $[Fe(OMe)_2(O_2CCH_2Cl)]_{10}$. The terminal H and Cl atoms have been excluded.

Figure 1b) Side view of $[Fe(OMe)_2(O_2CCH_2Cl)]_{10}$ with H and Cl atoms excluded.

Figure 2 Charge density $\rho(\vec{r})$ contours of the "ferric wheel" molecule on the plane of the Fe ring ($z = 0$). Contours are from 0.001 to 0.005 e/a_0^3, with intervals of 0.001 e/a_0^3, from 0.005 to 0.01 e/a_0^3 with intervals of 0.002 e/a_0^3 and from 0.01 to 0.1 e/a_0^3 with intervals of 0.02 e/a_0^3.

Figure 3: Spin density $[\rho_\uparrow(\vec{r}) - \rho_\downarrow(\vec{r})]$ contours of the "ferric wheel" molecule on the plane $z = 0$. Contours are from $\pm$ 0.0001 to $\pm$ 0.001 e/a_0^3 with interval 0.0004 e/a_0^3, from $\pm$ 0.001 to $\pm$ 0.01 e/a_0^3 with interval 0.002 e/a_0^3 and from $\pm$ 0.01 to $\pm$ 0.1 e/a_0^3 with interval 0.02 e/a_0^3. Full lines are positive values.

Figure 4: Total density of states (DOS) for $[Fe(OC)_2(O_2CC)]_{10}$. "Fermi level" has been shifted to zero energy.

Figure 5: Fe(3d) density of states for spin up (upper figure) and spin down (lower figure).

Figure 6a: Fe (4s) density if states for positive spin (upper figure) and negative spin (lower figure).

Figure 6b: Fe(4p) density of states for spin up (upper figure) and spin down (lower figure).

Figure 7: Partial view of two Fe atoms (large light spheres) with bridging Oxygens (small dark spheres) and Carbons (small light spheres).

Figure 8: Schematic representation of the projection on the plane of the Fe atoms ($z = 0$) of the direction of the field gradient V_{zz} at the Fe nuclei.

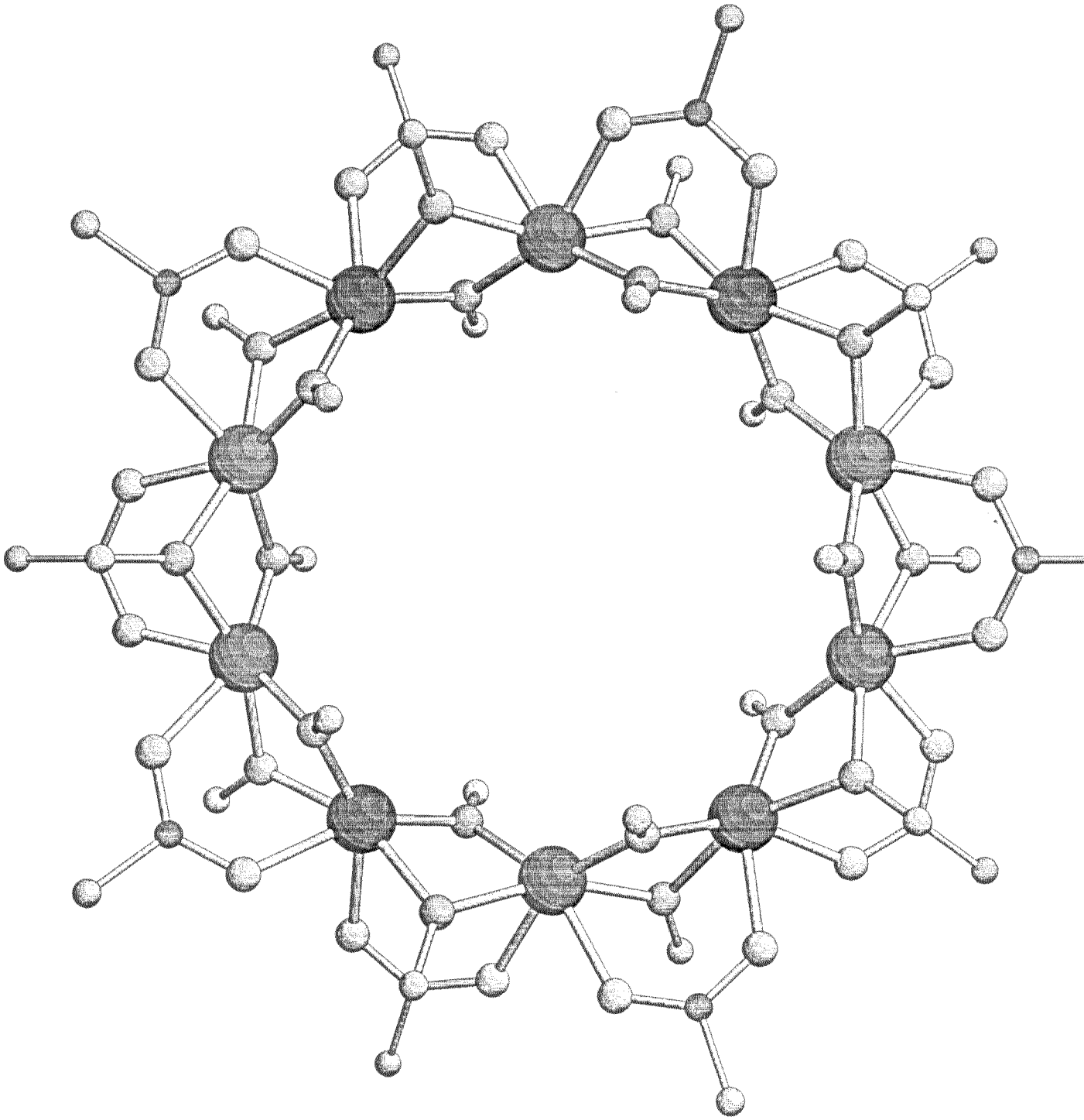

Fig. 1a

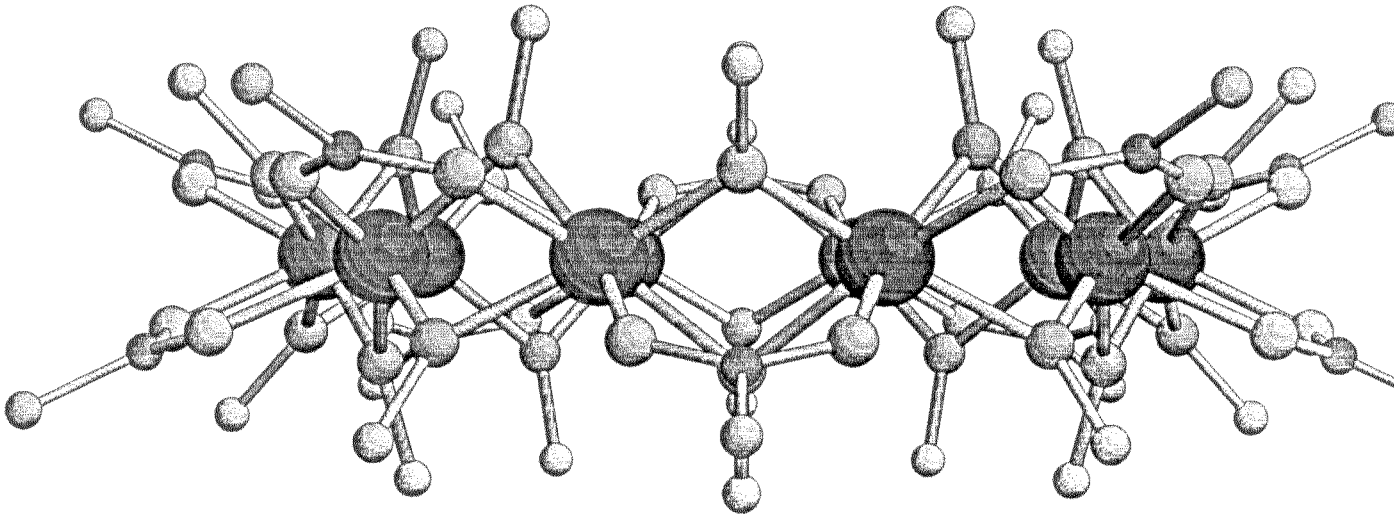

Fig. 1b

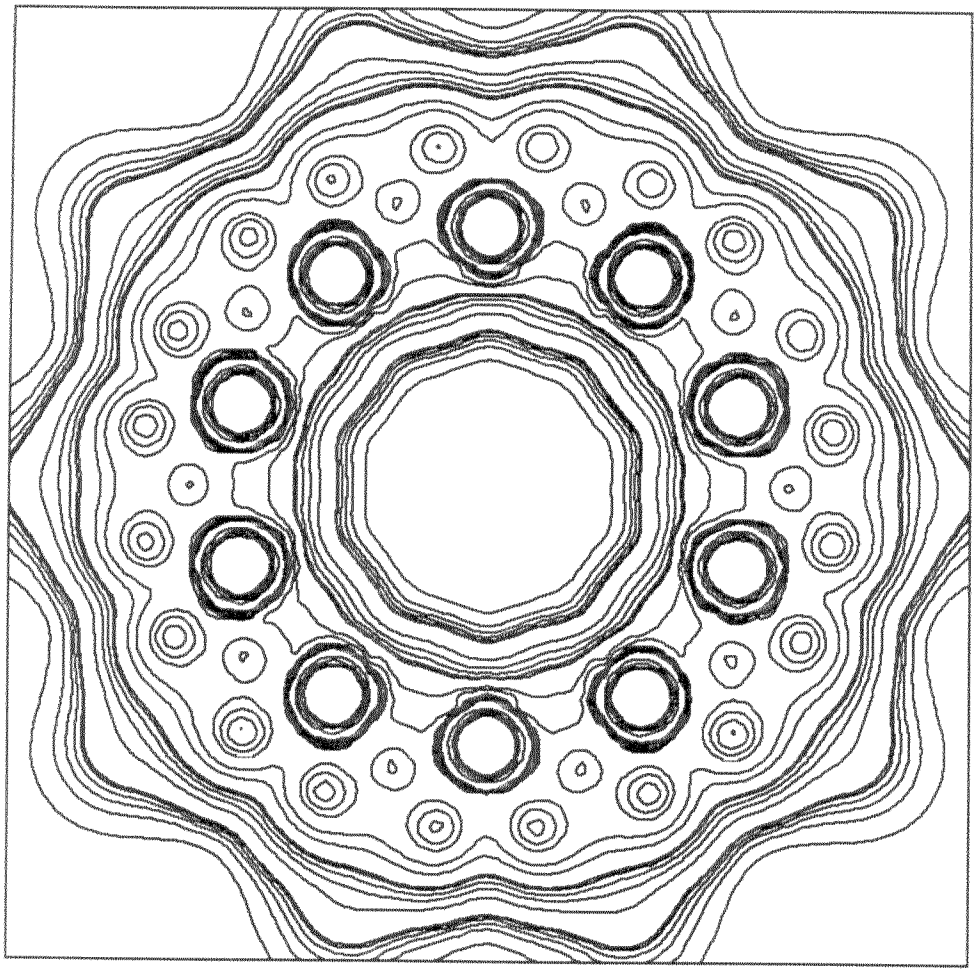

Fig. 2

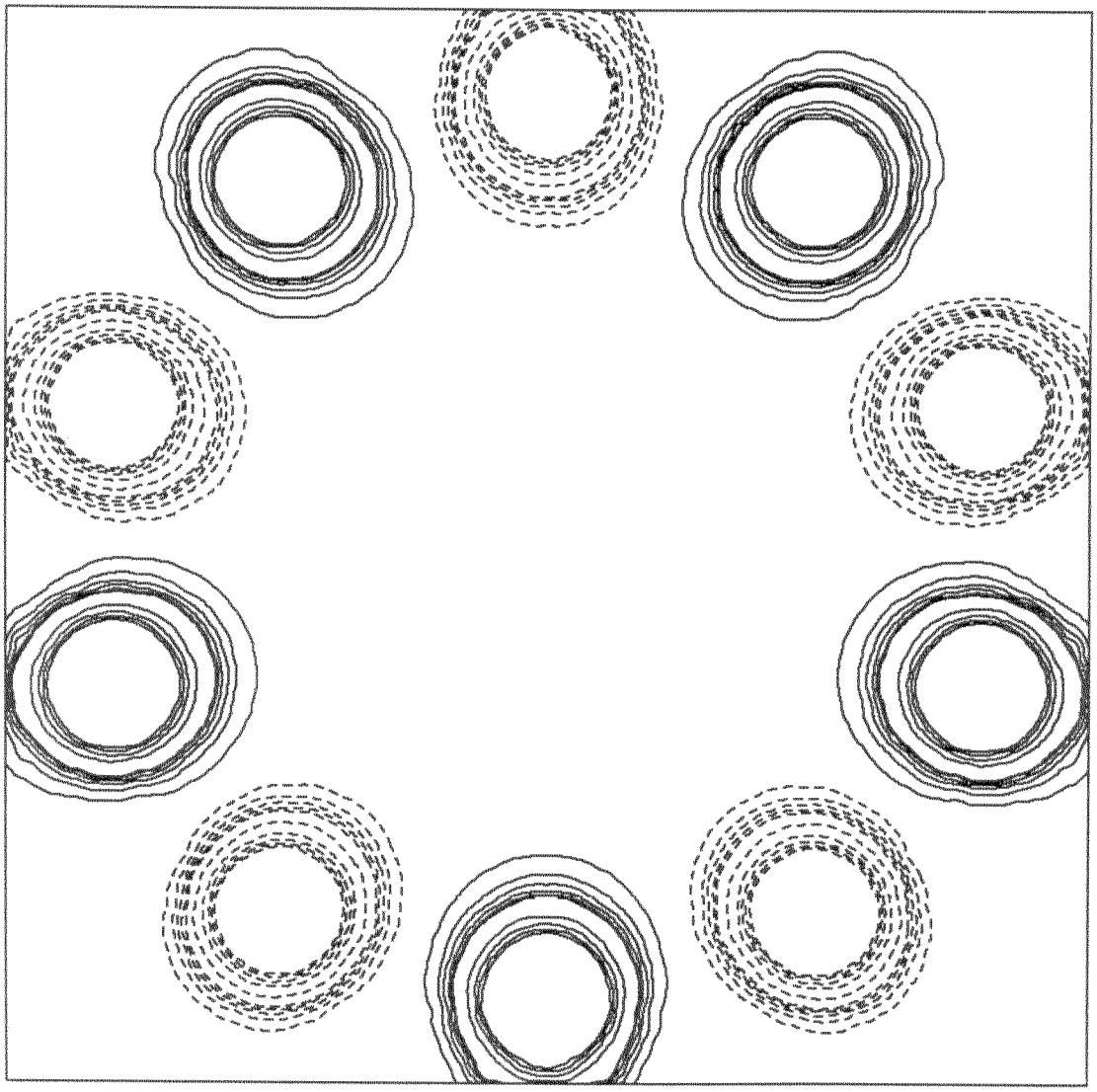

Fig. 3

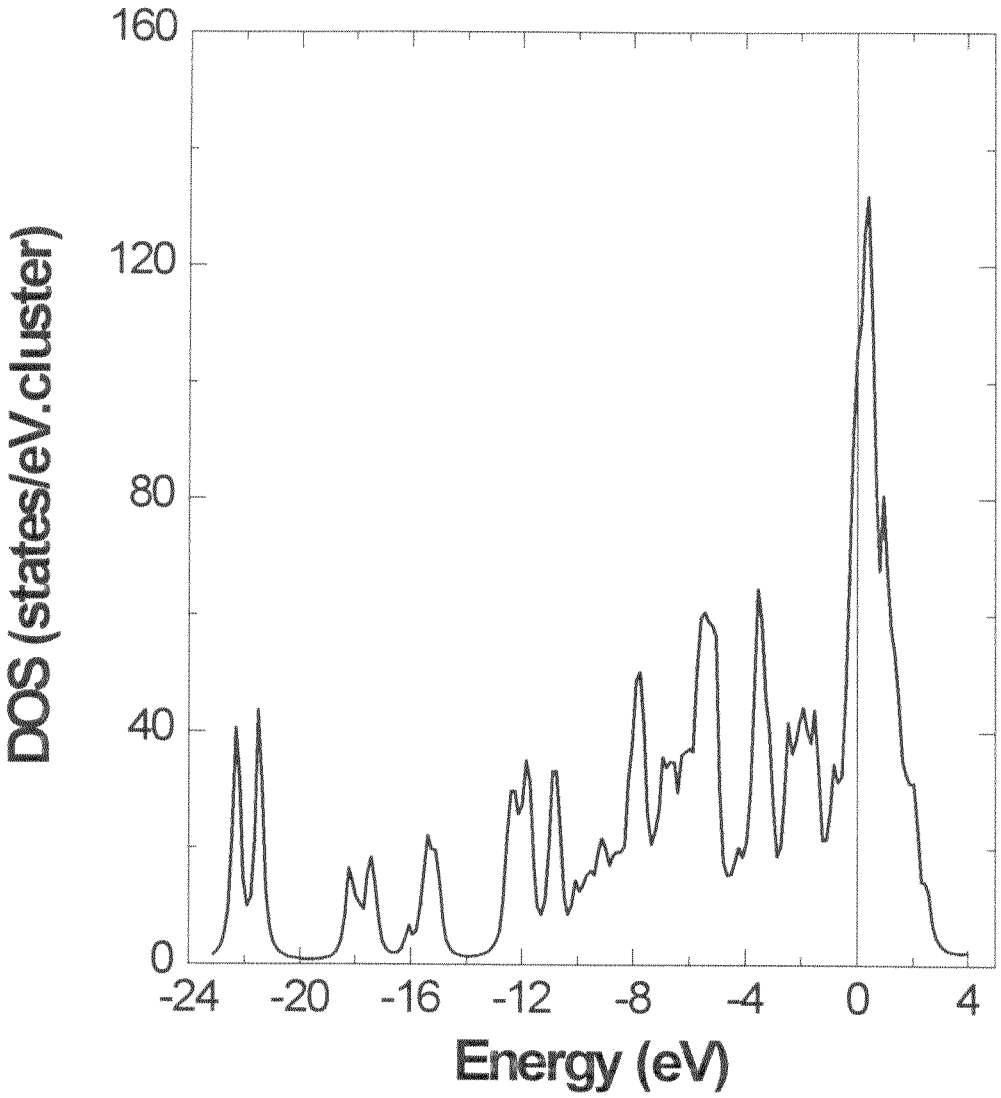

Fig. 4

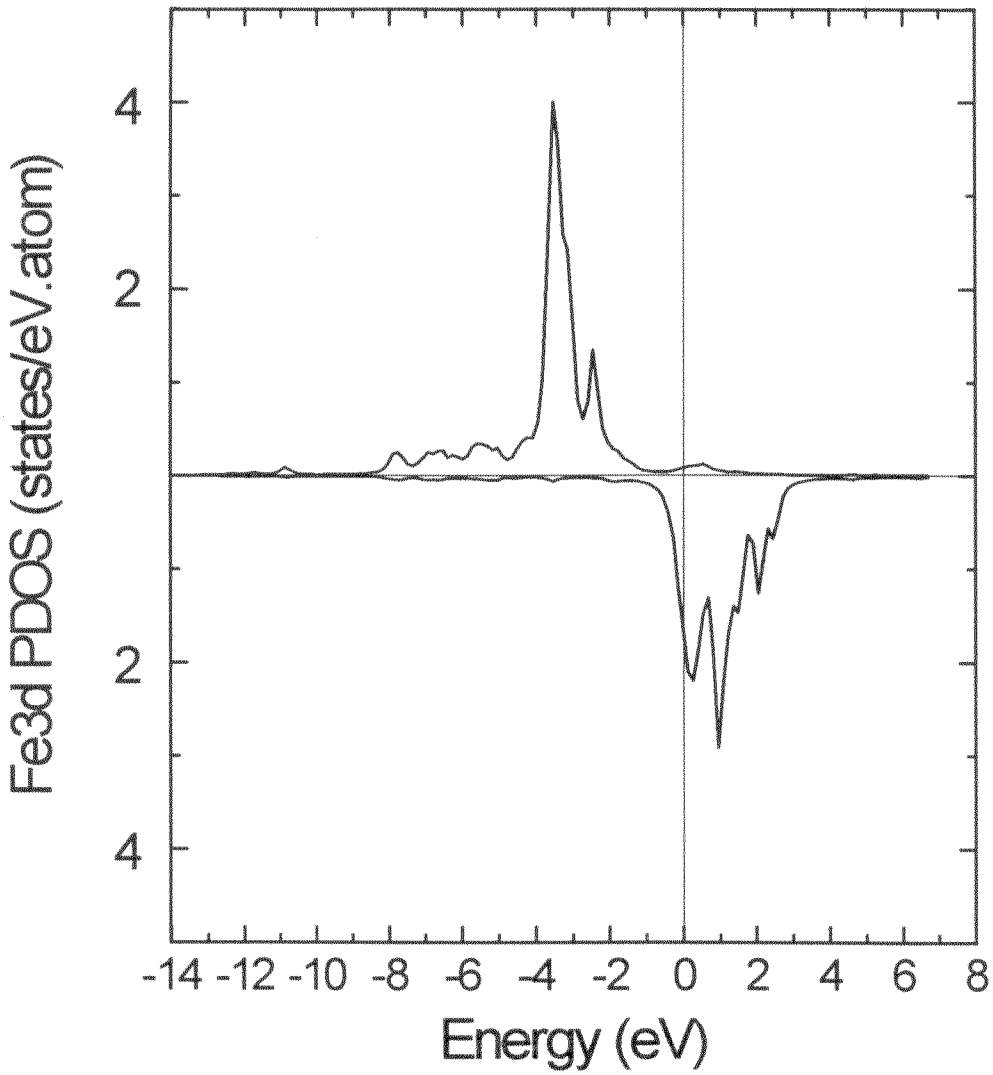

Fig. 5

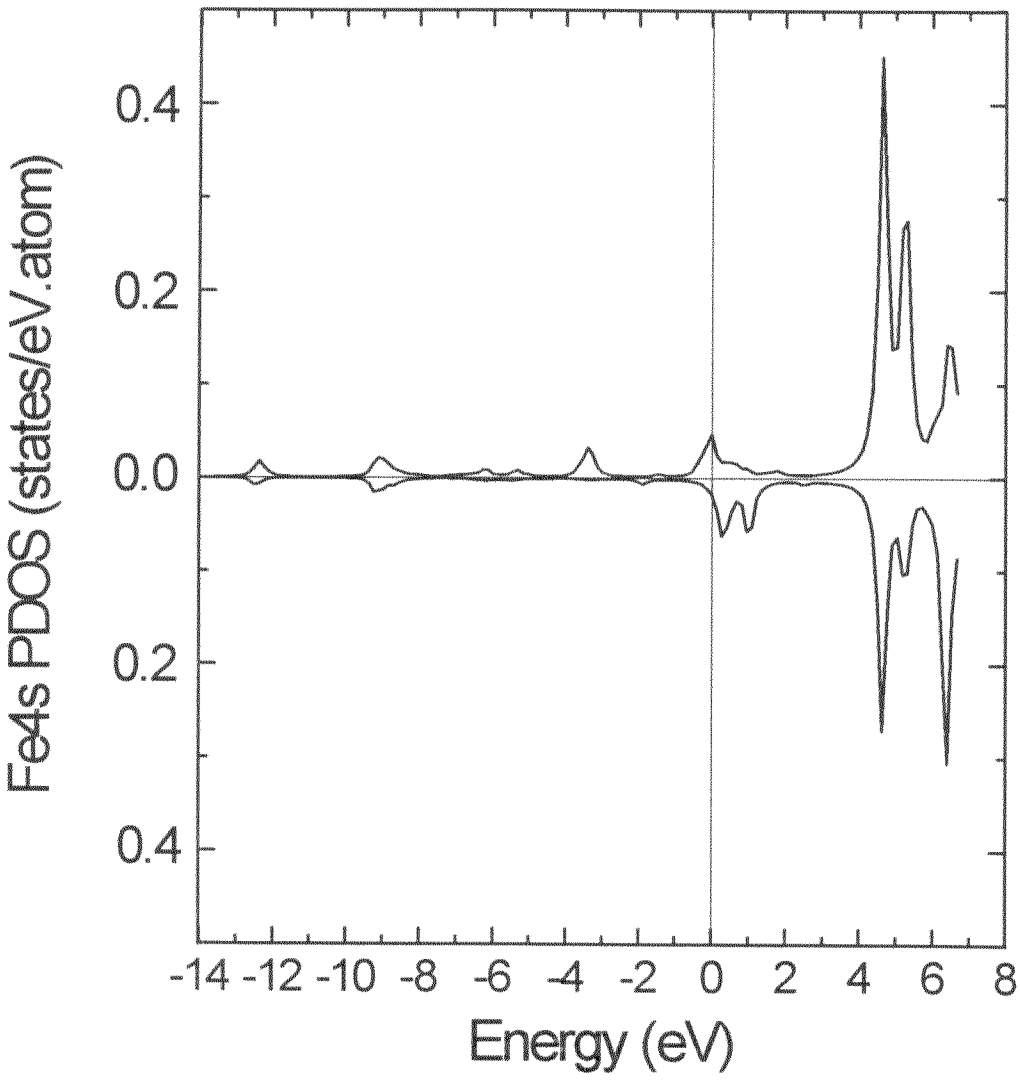
Fe4s PDOS (states/eV.atom)
0.4
0.2
0.0
0.2
0.4
-14 -12 -10 -8 -6 -4 -2 0 2 4 6 8
Energy (eV)

Fig. 6a

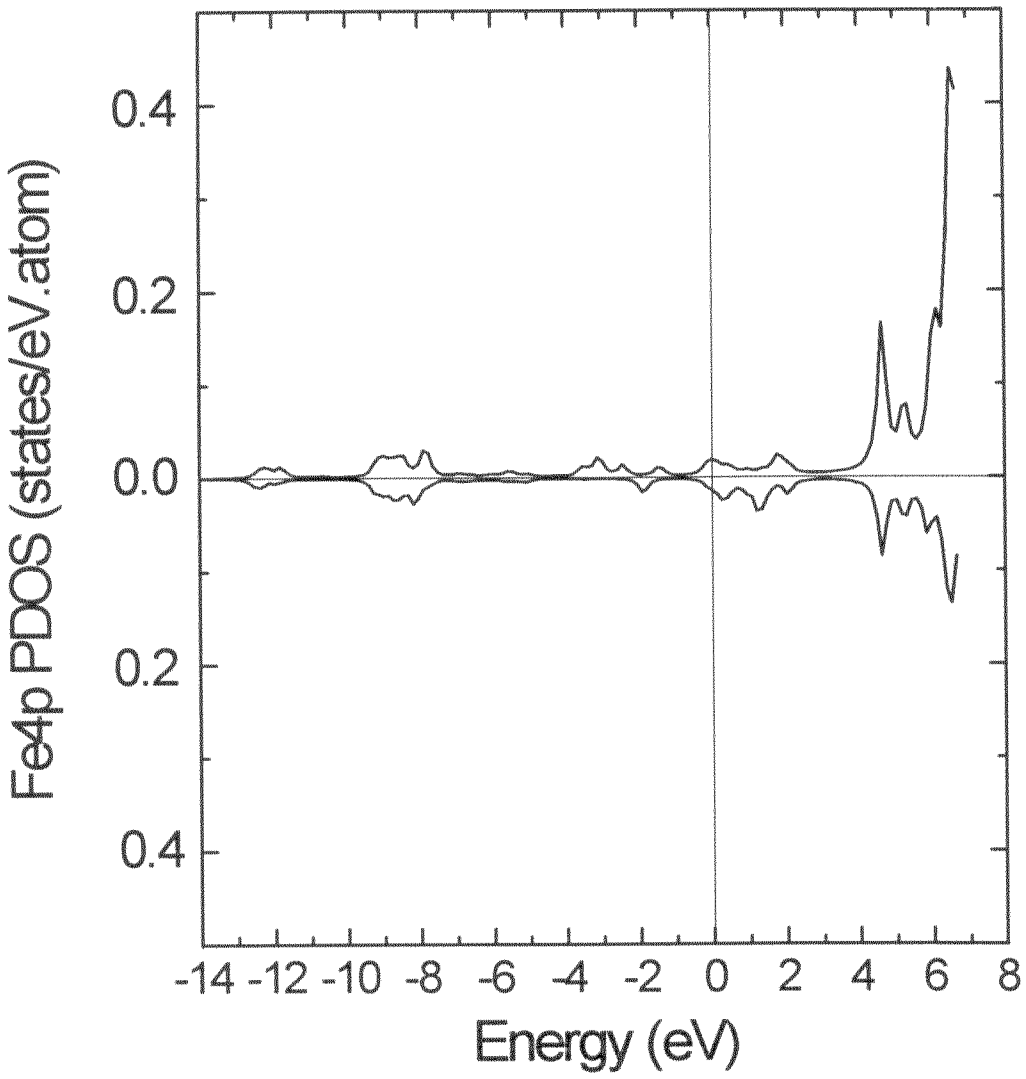
Fe4p PDOS (states/eV.atom)
0.4
0.2
0.0
0.2
0.4
-14 -12 -10 -8 -6 -4 -2 0 2 4 6 8
Energy (eV)

Fig. 6b

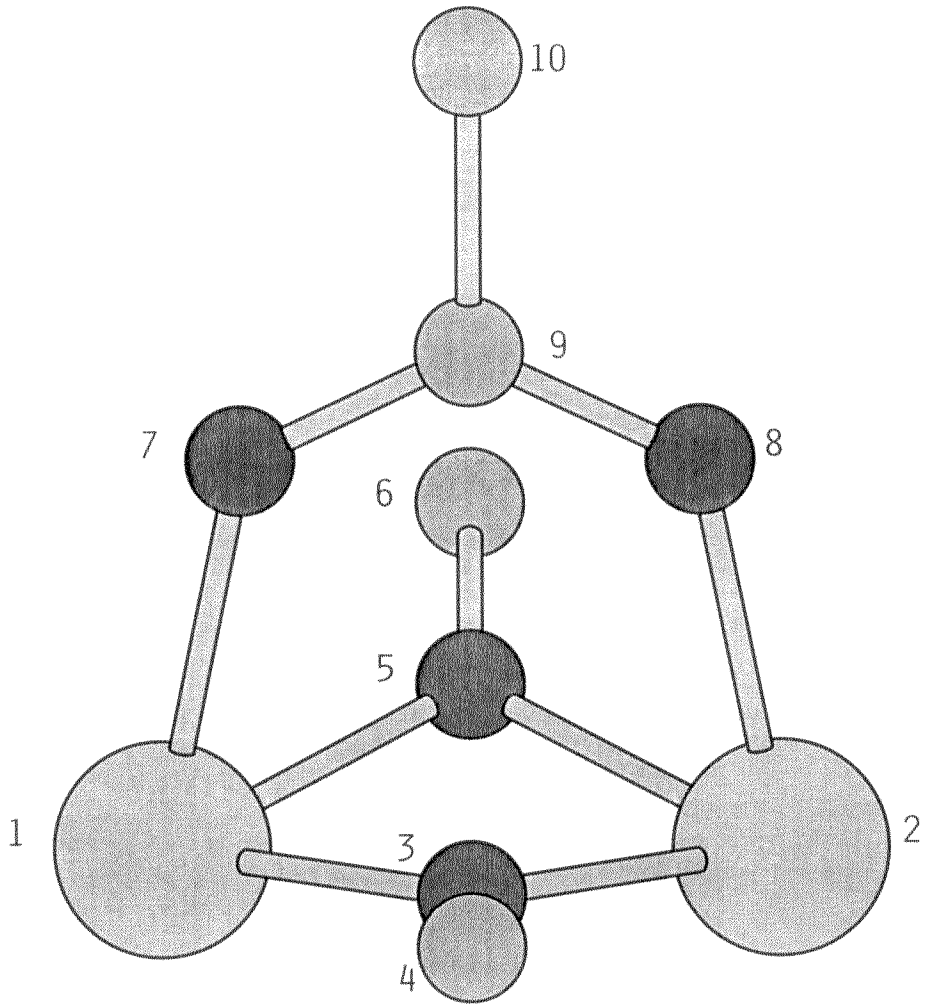

Fig. 7

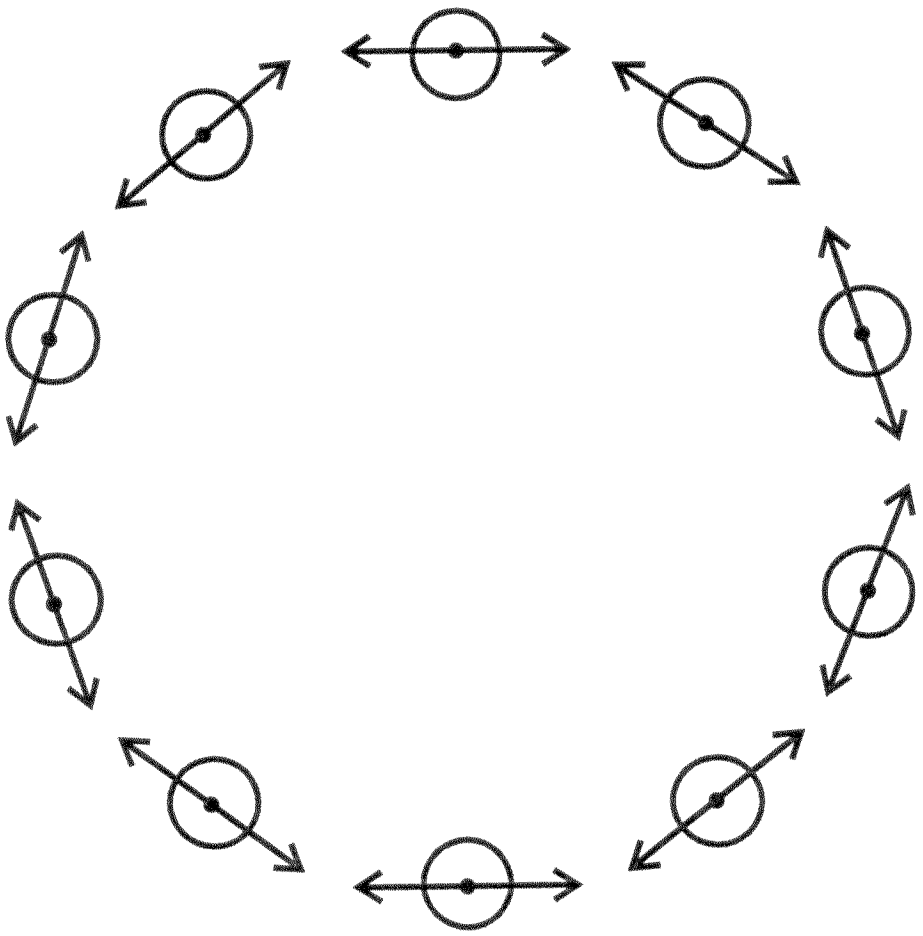

Fig. 8

References

[1] D.D. Awschalom and D.P. DiVincenzo, Physics Today **48**, 43 (1995).

[2] D.D. Awschalom, D.P. DiVincenzo and J.F. Smyth, Science **258**, 414 (1992).

[3] A.D. Kent, S. von Molnar, S. Gider and D.D. Awschalom, J. Appl. Phys. **76**, 6656 (1994).

[4] J.F. Smyth, S. Schultz, D.R. Fredkin, D.P. Kern, S.A. Rishton, H. Schmid, M. Cali and T.R. Koeler, J. Appl. Phys. **69**, 5262 (1991).

[5] R.F. Ziolo, E.P. Giannelis, B.A. Weinstein, M.P. O'Horo, B.N. Ganguly, V. Mehrotra, M.W. Russel and D.R. Huffman, Science **257**, 219 (1992).

[6] D.D. Awschalom, J.F. Smyth, G. Grinstein, D.P. DiVincenzo and D. Loss, Phys. Rev. Letters **68**, 3092 (1992); and references therein.

[7] F.C. Meldrum, B.R. Heywood and S. Mann, Science **257**, 522 (1992).

[8] D. Gatteschi, A. Caneshi, L. Pardi and R. Sessoli, Science **265**, 1054 (1994).

[9] K.L. Taft and S.J. Lippard, J. Am. Chem. Soc. **112**, 9629 (1990).

[10] K.L. Taft, C.D. Delfs, G.C. Papaefthymiou, S. Foner, D. Gatteschi and S.J. Lippard, J. Am. Chem. Soc. **116**, 823 (1994).

[11] G.C. Papaefthymiou, Phys. Rev. B**46**, 10366 (1992).

[12] C. Delfs, G. Gatteschi, L. Pardi, R. Sessoli, K. Wieghardt and D. Hanke, Inorg. Chem. **32**, 3099 (1993).

[13] A. Caneschi, A. Cornia, S.J. Lippard, G.C. Papaefthymiou and R. Sessoli, Inorganica Chimica Acta **243**, 295 (1996).

[14] A.K. Powell, S.L. Heath, D. Gatteschi, L. Pardi, R. Sessoli, G. Spina, F. Del Giallo and F. Pieralli, J. Am. Chem. Soc. **117**, 2491 (1995).

[15] D. Gatteschi, E. Sessoli, W. Plass, A. Müller, E. Krickemeyer, J. Meyer, S. Sölter and P. Adler, Inog. Chem. **35**, 1926 (1996).

[16] A. Bencini, C.A. Ghilardi, S. Midollini, A. Orlandini, U. Russo, M.G. Uytterhoeven and C. Zanchini, J. Chem. Soc. Dalton Trans. **1995**, 963.

[17] T.G. St. Pierre, D.H Jones and D.P.E. Dickson, J. Mag. Magn. Mat. **69**, 276 (1987).

[18] R. Sessoli, D. Gatteschi, A. Caneschi and M.A. Novak, Nature **365**, 141 (1993).

[19] R.D. Michael, R.D. Shull, L.J. Swartzendruber, L.H. Bennett and R.E. Watson, J. Mag. Magn. Materials **111**, 29 (1992).

[20] B. Barbara and E.M. Chudnovsky, Physics Letters A **145**, 205 (1990).

[21] D.E. Ellis and G.S. Painter, Phys. Rev. B **2**, 2887 (1970); D.E. Ellis, Int. J. Quant. Chem. **S2**, 35 (1968); E.J. Baerends, D.E. Ellis and P. Ros, Chem. Phys. **2**, 41 (1973); D.E. Ellis and J. Guo in "Electronic Density Functional Theory of Molecules, Clusters and Solids" ed. D.E. Ellis, Kluwer, Dordrecht (1994).

[22] see, for example: R.G. Parr and W. Yang, "Density Functional Theory of Atoms and Molecules", Oxford University Press, N. York (1989).

[23] V. von Barth and L. Hedin, J. Phys. C **5**, 1629 (1972).

[24] B. Delley and D.E. Ellis, J. Chem. Phys. **76**, 1949 (1982).

[25] C. Umrigar and D.E. Ellis, Phys. Rev. B **21**, 852 (1980).

[26] P.-L. Cao, D.E. Ellis and A.J. Freeman, Phys. Rev. B **25**, 2124 (1982).

[27] N.N. Greenwood and R.C. Gibb, "Mössbauer Spectroscopy", Chapman and Hall London (1971).

[28] "Mössbauer Isomer Shifts", eds. G.K. Shenoy and F.E. Wagner, North-Holland, Amsterdam (1978).

[29] J. Terra and D. Guenzburger, J. Physical Chem. **99**, 4935 (1995).

[30] D. Guenzburger and D.E. Ellis, Phys. Rev. B **22**, 4203 (1980).

[31] J. Terra and D. Guenzburger, Phys. Rev. B **44**, 8584 (1991).

[32] D. Guenzburger and D.E. Ellis, Phys. Rev. B **36**, 6971 (1987).

[33] P. Dufek, P. Blaha and K. Schwarz, Phys. Rev. Letters **75**, 3545 (1995).